International Journal of Nanoelectronics and Materials
IJNeaM
ISSN 1985-5761 | E-ISSN 2232-1535

# Synergistic electromagnetic wave absorbing properties of $NiFe_2O_4$/MWCNT composites synthesized via microwave-assisted combustion method in Ku-band

Mohd Hilmi Johari [a], Ismayadi Ismail [a] *, Rabaah Syahidah Azis [a,b], Chan Kar Tim [b], Nur Biha Mohamed Nafis [b], Mehmet Ertugrul [c], and Ibrahim Hakki Karakaş [d]

[a]*Nanomaterial Synthesis and Characterization Laboratory, Institute of Nanoscience and Nanotechnology (ION2), Universiti Putra Malaysia, 43400 Serdang, Selangor*
[b]*Department of Physics, Faculty of Science, Universiti Putra Malaysia, 43400 Serdang, Selangor, Malaysia*
[c]*Metallurgy and Materials Engineering, Karadeniz Technical University, Trabzon, 61080, Turkey*
[d]*Faculty of Engineering, Department of Food Engineering, Bayburt University, Bayburt, Turkey*
** Corresponding author. Tel.: +60369797546; e-mail: ismayadi@upm.edu.my*

Received 03 April 2024, Revised 13 June 2024, Accepted 05 September 2024

**ABSTRACT**

This study investigates the synthesis, microstructural characteristics, magnetic properties, and electromagnetic wave absorption performance of nickel ferrite ($NiFe_2O_4$) composites reinforced with multi-walled carbon nanotubes (MWCNTs) synthesized via the microwave-assisted combustion (MAC) method. X-ray diffraction (XRD) analysis confirmed the desired structure of $NiFe_2O_4$ and the successful integration of MWCNTs within the $NiFe_2O_4$ matrix. Field emission scanning electron microscopy (FESEM) analysis revealed the entanglement of MWCNTs and their significant impact on hindering particle growth, resulting in a finer particle structure. The reduction in average particle size from 1.317 µm for pure $NiFe_2O_4$ to 0.436 µm for $NiFe_2O_4$ with 2wt% MWCNT, representing approximately a 66.89% reduction, significantly demonstrates the effectiveness of MWCNTs in limiting particle growth and promoting a more refined particle structure. Magnetic property analyses showed a nuanced interplay between MWCNT concentration and composite behaviour, with the saturation magnetization ($M_s$) exhibiting substantial enhancement in the $NiFe_2O_4$/2wt%MWCNT composite, indicative of effective alignment of magnetic moments. However, a subsequent decrease in $M_s$ at higher MWCNT concentrations (4wt% and 6wt%) suggested potential dilution effects and disruptions in magnetic interactions within the composite. Electromagnetic wave absorption investigations revealed $NiFe_2O_4$/4wt%MWCNT as a highly efficient absorber in the Ku-band, with superior impedance matching and a high attenuation constant. The reflection loss (RL) reached a maximum of –17.58 dB at 12.78 GHz, signifying absorption of more than 99% of the incident EM wave in the microwave range. The favourable impedance matching and high attenuation constant contributed to the superior performance of $NiFe_2O_4$/4wt%MWCNT compared to pure $NiFe_2O_4$ and MWCNT. These findings suggest the potential of $NiFe_2O_4$/MWCNT composites for applications in telecommunications, aerospace, and electronics, with opportunities for further optimization and investigation into long-term stability and durability under varying environmental conditions.

**Keywords:** *$NiFe_2O_4$ nanoparticles, Microwave-assisted combustion method, Hybrid composites, Electromagnetic wave absorption, Multiwall carbon nanotubes (MWCNTs)*

## 1. INTRODUCTION

Microwave-absorbing materials (MAMs) play pivotal roles in both civilian and military domains by dissipating electromagnetic wave power through heat conversion. Low-frequency electromagnetic waves (EMWs) induce electrical noise in electronic devices, wireless communication systems, Bluetooth, and Wi-Fi applications, driving the imperative for electromagnetic interference (EMI) shielding. In military contexts, stealth technologies operate within high-frequency ranges such as X (8–12 GHz) and C (2–4 GHz) bands, further underscoring the critical need for effective MAMs. Desirable attributes for practical MAMs include low density, slender matching thickness, robust absorption, expansive absorption bandwidth, and cost-effectiveness.

The quest for efficient MAMs has been a cornerstone in advancing modern stealth technology, with a focus on materials capable of minimizing electromagnetic wave reflection while maximizing absorption. This pursuit has led to extensive research efforts aimed at understanding and manipulating the magnetic and dielectric properties of various materials to achieve optimal microwave absorption characteristics. Sahu *et al.*'s study on Sr-doped nano Ni-Co ferrite (NCFO) showcased the impact of dopant concentration on magnetic parameters, where the highest saturation magnetization ($M_s$) and optimal microwave absorption were achieved at specific doping levels, highlighting the importance of precise material engineering for efficient absorption. Their work revealed a notable improvement in microwave absorption, with a maximum reflection loss (RL) of –35.59 dB achieved at 17.74 GHz for the NCFO sample [1]. Nagasree *et al.*'s investigation into E-glass/epoxy composites blended with multi-walled carbon nanotubes (MWCNTs) and $Ni_{0.5}Zn_{0.5}Fe_2O_4$ nanopowder demonstrated the synergistic effects of

combining magnetic and dielectric components to address impedance mismatch issues, resulting in improved microwave absorption characteristics suitable for radar-absorbing structures (RAS). The work achieved a reflection loss of −16 dB for a two-layered RAS [2]. Aggarwal *et al.* exploration of zinc-substituted nickel spinel ferrites emphasized the significance of chemical composition and structure in achieving exceptional microwave absorption capabilities, with a low reflection loss (RL) of −31.17 dB achieved for a composition of x = 0.2 indicating efficient absorption [3]. Smitha *et al.*'s work on nanostructured nickel ferrite and nickel zinc ferrite highlighted the importance of impedance matching and multilayering techniques for broadband absorption, optimizing complex permittivity and permeability to minimize RL values, thus advancing the development of efficient EM wave-absorbing materials with reduced coating thickness. Their MAMs with broad bandwidth absorption and reduced coating thickness, achieved a reflection loss (RL) value of −45.0 dB for a moderately low coating thickness of 1.72 mm [4]. Finally, Ghodake's research on cobalt-substituted Ni-Zn ferrites elucidated the influence of cobalt content on magnetic properties and microwave absorption, with higher cobalt concentrations leading to enhanced absorption in specific frequency ranges, offering potential applications in radar systems. All their samples exhibited absorption in the frequency range of 2.3–2.5 GHz [5].

However, standalone dielectric and magnetic materials frequently exhibited subpar microwave absorption performance due to impedance mismatch issues. Consequently, the integration of magnetic and dielectric materials has emerged as a promising strategy to effectively match absorber impedances with free space. The integration of multi-walled carbon nanotubes (MWCNTs) with ferrites proved to be a valuable technique for enhancing the electromagnetic absorption characteristics of ferrite materials. According to research by Zhang *et al.* [6], the effectiveness of EM absorption was improved due to the formation of a hybrid conducting network inside the composite materials. This network resulted from the addition of graphene oxide, which increased the number of free electrons, functional groups, and defects available to interact with EM radiation. This caused the formation of electric dipoles that dissipated incident EM energy through relaxation losses. The addition of graphene oxide also enhanced electron hopping across the conductive network of MWCNTs and GO, leading to interfacial relaxation losses and converting more EM energy into heat energy. The hybrid structure also trapped maximum incoming EM radiation inside the various heterogeneous interfacial areas of nanosized ferrite particles functioning as magnetization centres and conductive MWCNT and GO networks acting as polarization centres [6]. By loading the surface of MWCNTs with ferrite nanoparticles and twinning them with graphene oxide, tiny current networks were created that increased conduction losses within the material.

Numerous methods have been developed for synthesizing spinel ferrite nanoparticles, including sol-gel, hydrothermal, combustion, precipitation, and aerosol techniques. However, these approaches often encounter drawbacks such as lengthy synthesis periods, complex procedures, expensive starting materials, and limited production capacities [7, 8]. Conversely, the microwave-assisted combustion (MAC) method offers distinct advantages, including cost-effectiveness, shortened reaction times, and scalability for large-scale production [8–10]. The combustion method is notable for its simplicity in chemical synthesis, facilitating rapid and safe production of metal oxide nanoparticles without the need for sophisticated equipment [11–13]. Unlike conventional methods, this technique incorporates a fuel substance into the system, typically organic compounds like glycine, urea, citric acid, or alanine, to enhance synthesis efficiency. Urea, specifically, is favoured for its affordability, abundance, safety, and non-toxicity [14, 15]. In the combustion process, metal nitrate salts are combined with the fuel at precise stoichiometric ratios, and the mixture is heated in a microwave oven to initiate exothermic reactions between the metal nitrates and urea. These reactions result in the formation of nanoparticles and/or agglomerates [16, 17]. Accurate temperature control is essential during this stage to prevent sintering and agglomeration, which can lead to an increase in the average particle size of the nanoparticles [15, 18]. In this study, nickel ferrite ($NiFe_2O_4$) nanoparticles were synthesized using the microwave-assisted combustion (MAC) method, a process that involved the formation of the precursor followed by auto-combustion. To achieve auto-ignition, a non-violent fuel like urea was used, which had the ability to release $CO_2$ and $H_2O$, resulting in an endothermic reaction with metal ions. Kothawale *et al.* [19] demonstrated the successful preparation of nickel zinc ferrite at low temperatures via the MAC method using a domestic microwave oven. Another recent study by Sami and Sadeq [20] used the microwave-assisted combustion technique to synthesize mixed spinel $Mg_{1-x}Zn_xFe_2O_4$ ferrite, with x ranging from 0 to 0.6. The method is quick, simple, and commonly performed in a solution medium, allowing for efficient synthesis of ferrite materials.

This investigation aims to bridge the gap between the inherent properties of ferrites and the pressing need for highly efficient MAMs through the incorporation of carbon nanotubes (CNTs). By leveraging the distinctive characteristics of both constituents, this amalgamation seeks to significantly enhance absorption performance while mitigating challenges associated with impedance matching. The hybridization of ferrites and CNTs presents a compelling avenue for achieving broad absorption bandwidths and robust absorption capacities across Ku-band frequency. Employing the MAC method could facilitate precise control over the microstructural features of the composite materials. Many literatures have reported on the use of nickel ferrites and MWCNT as filler materials for EM wave absorbers, however to the best of our knowledge, the hybridization of $NiFe_2O_4$ and MWCNT via MAC method using low-cost microwave oven and used as MAMs has yet been reported. Therefore, the main goal of this investigation is to examine the production of a hybrid substance utilizing $NiFe_2O_4$ and MWCNT via the MAC technique to achieve efficient MAMs. Our focus is to assess how the concentration

of MWCNT affects the performance of EM wave absorption of this hybrid material.

## 2. METHODOLOGY

### 2.1. Materials

This study employed nitrate salts of iron and nickel along with urea as fuel to synthesize nickel ferrite nanoparticles using the microwave-assisted combustion method. The metal sources used were Nickel (II) nitrate hexahydrate $Ni(NO_3)_2.6H_2O$ and ferric nitrate nonahydrate $Fe(NO_3)_3.9H_2O$ which were obtained from Sigma-Aldrich. Multiwall carbon nanotubes (MWCNTs) (Figure 1(a)) were self-prepared by the chemical vapour deposition (CVD) method (reported elsewhere [21] and mixed during the MAC method. In this study, the catalyst employed in the synthesis of MWCNTs was not removed after synthesis [21]. We utilized the MWCNTs directly as synthesized, foregoing any purification steps, as the residual catalyst particles enhance the electromagnetic properties of the composites. These metallic inclusions are vital, boosting the magnetic properties of the MWCNTs, which is essential for the electromagnetic wave absorption performance investigated in our research.

### 2.2. Synthesis of $NiFe_2O_4$/MWCNT Hybrid Composites

In this study, the MAC method was utilized to synthesize spinel nickel ferrite nanoparticles. The metal sources used were nickel (II) nitrate and iron (III) nitrate, which were weighed in a ratio of 1:2, corresponding to 3.325 g (mol) and 6.65 g (mol), respectively. The fuel reagent used was urea, which was weighed at 10.0 g based on the stoichiometric equation derived from the total mass of nickel (II) nitrate and iron (III) nitrate. The chemical equation for the synthesis of spinel nickel ferrite nanoparticles using the MAC method can be represented as Equation (1):

$$2Ni(NO_3)_2 + Fe(NO_3)_3 + 4CO(NH_2)_2 \rightarrow NiFe_2O_4 + 4CO_2 + 6H_2O + N_2 \quad (1)$$

The stoichiometric ratio of the metal sources (nickel nitrate and iron nitrate) and the fuel reagent (urea) is based on the molar amounts. The combustion of the mixture results in the formation of nickel ferrite nanoparticles along with the release of carbon dioxide, water, and nitrogen gas. To synthesize the nickel ferrites, metal salts and urea were mixed and stirred, resulting in the creation of a gel-like solution. No water was added during the stirring. The solution was then subjected to 800 W of microwave radiation in a kitchen-type microwave oven for about 5 minutes, leading to rapid combustion and the formation of a solid powder that was dark in colour. Prior to placing the gel-like solution in the microwave oven, a specific weight percentage of MWCNTs was added to it in order to prepare the $NiFe_2O_4$/MWCNT hybrid. The study utilized five samples: $NiFe_2O_4$, $NiFe_2O_4$/2wt%MWCNT, $NiFe_2O_4$/4wt% MWCNT, $NiFe_2O_4$/6wt%MWCNT, and pure MWCNT. After the synthesis process was complete for all of the samples, they were ground to a fine powder for at least 15 minutes and then subjected to XRD analysis to investigate their phase formation. The samples were analyzed using the Phillips XRD machine (Pw 3040/60 Mpd X'pert High Pro Panalytical Diffractometer), with copper, Cu Kα radiation at 40 kV and 30 mA of input current. The magnetic characteristics of the samples were investigated using a vibrating sample magnetometer (VSM, LakeShore Model 7407). The morphology of the samples was observed using the FeSEM NOVA Nanosem 230 and Transmission Electron Microscopy (TEM) (LEO 912AB Energy Filter). Additionally, the prepared samples were measured using a Vector Network Analyzer (VNA, model: N5227A PNA Network Analyzer) within the frequency range of 12 to18 GHz (Ku-band) with 3-mm thickness.

## 3. RESULTS AND DISCUSSION

### 3.1. Phase and Microstructural Analysis

X-ray diffraction (XRD) analysis was performed on both $NiFe_2O_4$ and $NiFe_2O_4$/MWCNT hybrids. The XRD patterns revealed that all peaks were indexed to $NiFe_2O_4$, indicating the successful synthesis of spinel nickel ferrite nanoparticles (Figure 1(b)). The indexed peaks at 2θ values of 30.31°, 35.70°, 37.34°, 43.39°, 53.84°, 57.40°, and 63.04° correspond to specific crystallographic planes of $NiFe_2O_4$. However, a peak at 2θ = 44.35° with the hkl index of (011) was observed, which is identically indexed to iron (Fe) with ICSD card no. 98-002-1576. This presence of Fe peaks in $NiFe_2O_4$ can be attributed to the incomplete chemical reaction during the synthesis process, as the short duration (5 minutes) and high power (850 watts) of microwave radiation might not have allowed for complete conversion to pure $NiFe_2O_4$.

The XRD spectra of $NiFe_2O_4$/MWCNT hybrids showed matching peaks of MWCNT carbon structure and $NiFe_2O_4$ patterns (Figure 1(b)). The diffraction peak at 2θ = 26.6° with the hkl index of (002) corresponds to the characteristic (002) plane of the MWCNT structure [22]. Additional carbon peaks were located at 2θ = 43.19°, 57.30°, and 62.95°, further confirming the presence of MWCNTs in the hybrid composite. The observation of MWCNT peaks confirms the successful synthesis of the $NiFe_2O_4$/MWCNT hybrid, where the MWCNTs are integrated into the $NiFe_2O_4$ matrix.

The MAC method utilizes microwave radiation to induce rapid combustion of the precursor materials. The fuel reagent, urea, acts as a combustion source, generating high temperatures and a highly reactive environment. The exothermic combustion reaction provides the necessary energy for the synthesis process. Microwave radiation directly interacts with polar molecules, such as water and metal salt ions, through dipolar rotation and ionic conduction. The oscillating electric field of microwaves causes the charged particles to align and reorient rapidly, generating heat. Microwave heating is highly efficient and uniform, facilitating the rapid synthesis of the desired materials. The metal sources, nickel (II) nitrate and iron (III) nitrate, undergo chemical reactions during the MAC

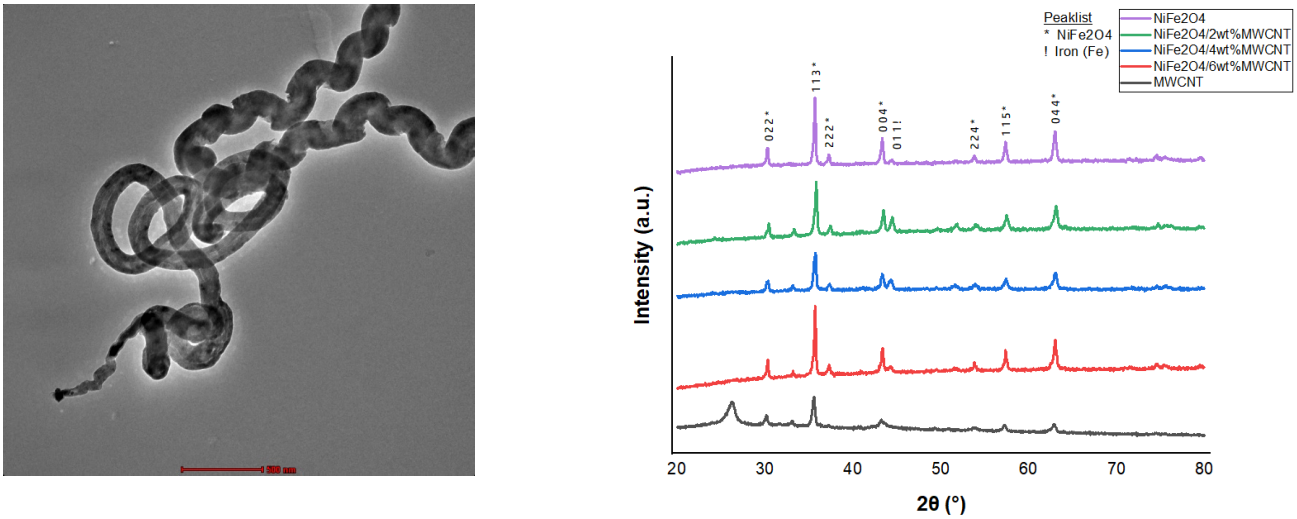


**Figure 1**. (a) Transmission electron microscope (TEM) image showing MWCNT prior to MAC method synthesis. (b) XRD patterns of pure $NiFe_2O_4$, pure MWCNT, and $NiFe_2O_4$/MWCNT with different concentrations of MWCNT of 2wt%, 4wt% and 6wt%

method. The metal salts react with the fuel reagent (urea) in the gel-like solution. The exothermic combustion releases energy, enabling the reduction and oxidation reactions to occur simultaneously, leading to the formation of nickel ferrite nanoparticles. Nickel ferrite ($NiFe_2O_4$) belongs to the spinel structure, where metal cations occupy tetrahedral (A) and octahedral (B) sites within the crystal lattice. The spinel structure is characterized by the arrangement of oxygen ions in a cubic close-packed (CCP) arrangement. The crystallographic planes indexed in the XRD patterns represent the specific arrangement of atoms within the spinel lattice.

The incomplete chemical reaction during the short synthesis duration and high power of microwave radiation can be explained by looking at the reaction kinetics and temperature effects. During the synthesis process, the chemical reaction between the metal salts (nickel and iron nitrates) and the fuel reagent (urea) is driven by the application of microwave radiation. Microwave heating utilizes electromagnetic waves that induce molecular motion and generate heat through dipolar rotation and ionic conduction. The short synthesis duration of 5 minutes limits the reaction time available for the chemical transformation to occur completely. The reaction kinetics, which describes the rate at which reactants are converted into products, depends on factors such as temperature, concentration, and reaction pathways. In this case, the rapid and intense heating caused by the high power of 850 watts promotes a fast reaction rate. However, the limited duration may not allow for sufficient time for all iron ions to undergo complete conversion into the desired $NiFe_2O_4$ phase. As a result, some iron ions remain unreacted or partially reacted, leading to the coexistence of Fe impurities in the final product.

The high power of microwave radiation, in conjunction with the short duration, can also have temperature-related effects. The rapid and intense heating can cause a localized increase in temperature within the reaction mixture. However, the temperature distribution and heat transfer throughout the sample may not be uniform, leading to thermal gradients. These thermal gradients can result in uneven heating and variations in the reaction progress across the sample. Some regions may reach higher temperatures, favouring faster reaction rates, while others may experience lower temperatures and slower reactions. Consequently, the overall conversion of iron ions to $NiFe_2O_4$ may be limited by the localized temperature conditions, further contributing to the presence of Fe impurities.

To achieve a higher degree of phase purity in the synthesized $NiFe_2O_4$ material, further optimization of the synthesis conditions is recommended. This may involve extending the reaction duration to provide more time for complete conversion and allowing the diffusion of ions to occur more uniformly. Additionally, lowering the power settings of the microwave radiation can help minimize the formation of thermal gradients, ensuring a more homogeneous distribution of temperature and facilitating a more complete reaction throughout the sample. By optimizing these parameters, it is possible to enhance the reaction kinetics and temperature conditions, ultimately leading to a higher degree of phase purity in the final $NiFe_2O_4$ product.

The XRD patterns of $NiFe_2O_4$/MWCNT hybrids show matching peaks of MWCNT carbon structure and $NiFe_2O_4$, indicating the successful synthesis of the hybrid composite. The presence of MWCNT peaks confirms the integration of carbon nanotubes within the $NiFe_2O_4$ matrix. The interaction between the MWCNTs and the $NiFe_2O_4$ phase can be attributed to the dispersion and entanglement of MWCNTs during the synthesis process, providing a network structure within the composite material. The interaction between multiwalled carbon nanotubes (MWCNTs) and the $NiFe_2O_4$ phase in the hybrid composite can be understood through the dispersion, entanglement, and the formation of a network structure. During the synthesis process, the MWCNTs are introduced into the gel-like solution

containing the metal salts and urea. As the solution undergoes the synthesis reaction and subsequent combustion, the MWCNTs disperse and distribute within the mixture. This dispersion is facilitated by various factors, including the stirring action and the surface properties of the MWCNTs. The dispersion of MWCNTs allows for their integration into the $NiFe_2O_4$ matrix. As the synthesis reaction progresses, the MWCNTs become surrounded and embedded within the growing $NiFe_2O_4$ nanoparticles. This integration occurs due to intermolecular forces, such as van der Waals interactions, between the MWCNTs and the surrounding $NiFe_2O_4$ molecules. The entanglement of MWCNTs within the composite material further enhances the interaction between MWCNTs and the $NiFe_2O_4$ phase. The entanglement occurs as a result of the complex three-dimensional network structure formed by the overlapping and intertwining of individual MWCNTs. The entangled MWCNTs create a network that extends throughout the $NiFe_2O_4$ matrix, enhancing the interfacial contact and interlocking between the two components. The presence of MWCNT peaks in the XRD patterns confirms the successful synthesis of the $NiFe_2O_4$/MWCNT hybrid composite and suggests that the MWCNTs maintain their structural integrity within the composite material. The matching peaks of the MWCNT carbon structure and the $NiFe_2O_4$ phase indicated that the MWCNTs are dispersed and integrated within the $NiFe_2O_4$ matrix rather than being agglomerated or forming separate phases. It is known that XRD provides foundational evidence of phase compatibility and structural cohesion. The observation of matching diffraction peaks corresponding to both the MWCNT carbon structure and the $NiFe_2O_4$ phase indicated a uniform dispersion and integration of MWCNTs within the $NiFe_2O_4$ matrix. This uniformity is evidenced by the absence of new or shifted peaks, which typically signify phase separations or structural distortions. Furthermore, the consistency of the diffraction peaks, without evidence of broadening or splitting, suggests no physical separation or inadequate integration, supporting the conclusion of a well-synthesized composite. Additional morphological results (Figures. 1(a), 2(a–b) and 3(a–e)) provided further confirmation of the MWCNTs' dispersion and interaction within the $NiFe_2O_4$ matrix.

The dispersion, integration, and entanglement of MWCNTs within the $NiFe_2O_4$ matrix contribute to the formation of a network structure within the composite material. This network structure enhances the overall properties of the hybrid composite by providing pathways for electron transport, improving mechanical strength, and potentially influencing magnetic behaviour. The interconnected MWCNT network can facilitate the transfer of charges and promote conductivity, while also reinforcing the structural integrity of the composite.

Figure 2(a–e) presents the FESEM morphologies and particle size distributions of the hybridization of MWCNT with nickel ferrite samples synthesized at different concentrations of MWCNT. The nickel ferrite sample exhibits an average grain size of 1.317 μm, with some nickel ferrite nanoparticle grains showing irregular-shaped spherical structures, while others exhibit a cubic-like structure. When adding 2wt% MWCNT to the nickel ferrite nanoparticles, Figure 2(b) shows the presence of a curly structure in the MWCNT. The microstructure reveals a well-dispersed MWCNT with minimal agglomeration. We calculated the average grain size as 0.436 μm using the ImageJ software based on a particle distribution analysis of 200 particles. Moreover, at the concentration of 4wt% MWCNT, Figure 2(c) demonstrates an increased presence of the curly structure, along with successful hybridization of nickel ferrite on the outer wall of MWCNT. We observed an average grain size of 0.243 μm, and well-textured grains are visible. Figure 2(d) illustrates the attachment of grains in the $NiFe_2O_4$/6wt%MWCNT sample, resulting in agglomeration throughout the image. Upon observing the microstructure, it is apparent that the sample exhibits larger grain sizes, measuring 0.270 μm, in comparison to the grains observed in the $NiFe_2O_4$/4wt%MWCNT sample (Figure 2(c)). We observed the presence of curly-like and twisted fibre microstructures of MWCNT with an average grain size of 0.363 μm (Figure 2(e)). Table 1 provides a summary of the average grain sizes for each of the samples.

Pure $NiFe_2O_4$ exhibits a relatively larger average grain size of 1.317 μm (Table 1). The diameter of the MWCNTs used ranges from 20 to 160 nm, as detailed in reference [21]. The synthesis method and growth conditions during formation contribute to this size. The larger grain sizes can be attributed to the kinetics of growth and nucleation processes involved in the formation of $NiFe_2O_4$ nanoparticles.

**Table 1.** Average grain size, saturation magnetization, *Ms*, coercivity, *Hc* and Retentivity, *Mr* of pure $NiFe_2O_4$, MWCNT and $NiFe_2O_4$/MWCNT with different concentrations of MWCNT of 2wt%, 4wt% and 6wt%

| Sample Name | Average grain size (μm) | Saturation Magnetization, *Ms* (emu $g^{-1}$) | Coercivity Force, *Hc* (G) | Retentivity, *Mr* (emu $g^{-1}$) |
|---|---|---|---|---|
| $NiFe_2O_4$ | 1.317 | 36.293 | 132.80 | 8.1505 |
| $NiFe_2O_4$/2wt%MWCNT | 0.436 | 38.191 | 172.21 | 6.6954 |
| $NiFe_2O_4$/4wt%MWCNT | 0.243 | 36.090 | 162.55 | 7.0781 |
| $NiFe_2O_4$/6wt%MWCNT | 0.270 | 30.554 | 155.24 | 6.1928 |
| MWCNT | 0.363 | 10.694 | 157.01 | 2.0848 |

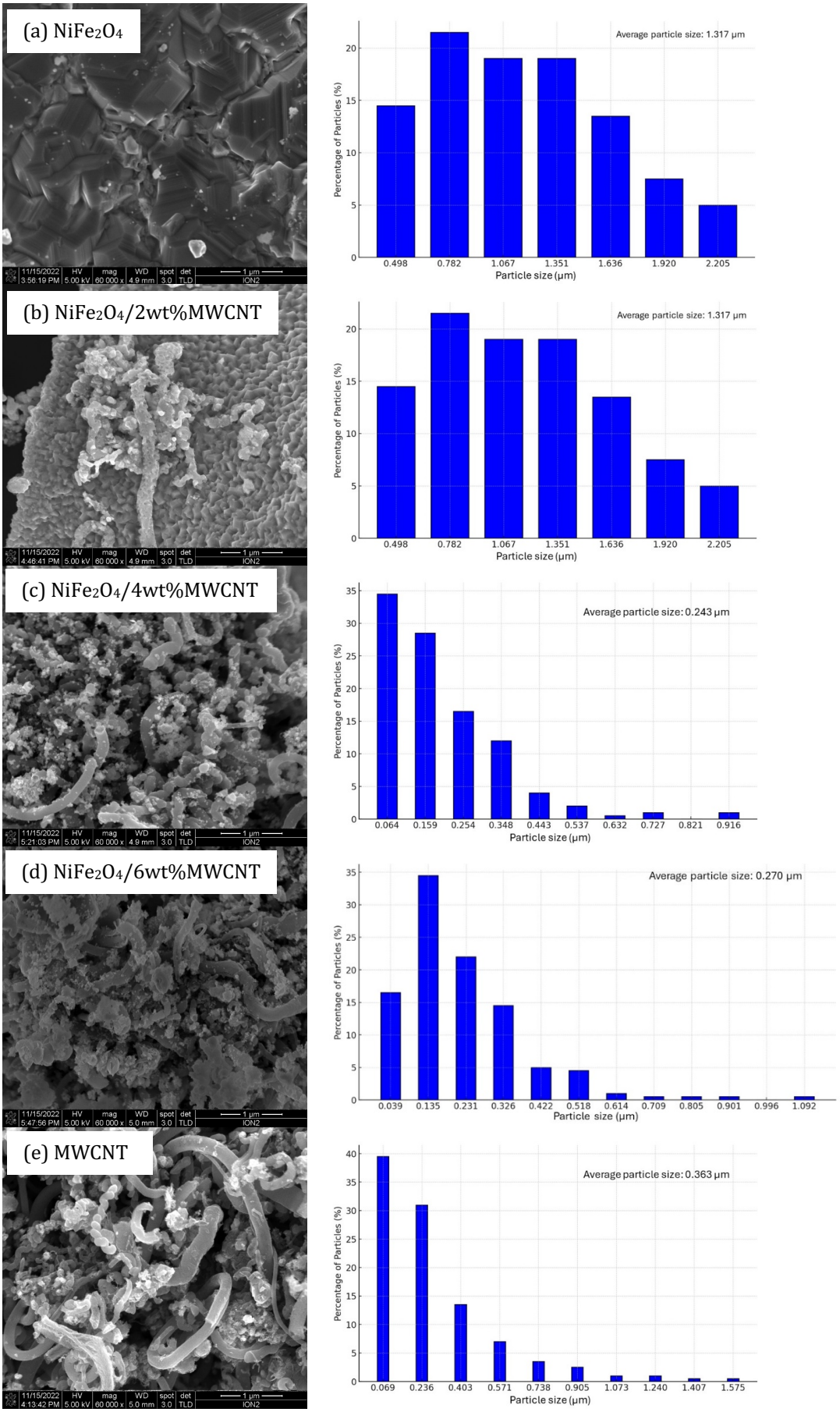


**Figure 2**. FESEM images and particle distribution of (a) $NiFe_2O_4$ (b) $NiFe_2O_4$/2wt%MWCNT, (c) $NiFe_2O_4$/4wt%MWCNT, (d) $NiFe_2O_4$/6wt%MWCNT, and (e) MWCNT

Incorporating MWCNTs into the $NiFe_2O_4$ matrix at a concentration of 2wt% leads to a significant reduction in the average grain size to 0.436 μm. This decrease in grain size can be attributed to the addition of MWCNTs, which serve as nucleation sites for the growth of $NiFe_2O_4$ nanoparticles. The presence of MWCNTs provides additional surfaces for crystal growth, resulting in the formation of smaller grains.

As the concentration of MWCNTs increases to 4wt% and 6wt% in the $NiFe_2O_4$/MWCNT hybrid composites, further reduction in grain size is observed. The average grain sizes decrease to 0.243 μm and 0.270 μm, respectively. This trend indicates that higher concentrations of MWCNTs promote the formation of even smaller grains in the composite material. The increased density of MWCNTs creates more nucleation sites, leading to enhanced grain refinement.

The grain size reduction in the presence of MWCNTs involves the interaction between the MWCNTs and the $NiFe_2O_4$ matrix. The MWCNTs can act as heterogeneous nucleation sites, providing templates for the growth of $NiFe_2O_4$ nanoparticles. The MWCNTs act as heterogeneous nucleation sites, offering templates for the growth of $NiFe_2O_4$ nanoparticles and influencing the crystallization process by modifying the local chemical environment and surface energies. This local chemical environment around the $NiFe_2O_4$ nanoparticles, shaped by the MWCNTs' unique surface chemistry featuring functional groups, defects, and inherent electronic properties, enhances the adsorption of metal ions on the surface of MWCNTs. This facilitation aids the nucleation and subsequent growth of $NiFe_2O_4$ nanoparticles, where the rate of ion deposition and nucleation kinetics directly impact the crystalline structure and purity. Meanwhile, the high surface energy of the MWCNTs promotes increased nucleation rates and more homogeneous nucleation across the carbon nanotube surfaces, crucial for achieving uniform grain sizes and shapes in the synthesized composites. Additionally, the presence of MWCNTs can hinder grain growth by pinning and impeding the movement of grain boundaries, affecting the overall grain growth and size distribution. Additionally, the presence of MWCNTs can hinder grain growth through pinning and impeding the movement of grain boundaries. The entanglement and dispersion of MWCNTs within the matrix create obstacles for grain boundary migration, leading to a finer grain structure [23, 24]. The XRD patterns (Figure 1(b)) and microscopic images (Figures 2(a–e)) demonstrated no additional peaks or significant peak shifts, suggesting no unreacted $NiFe_2O_4$ or MWCNTs and confirming successful integration. The images clearly show $NiFe_2O_4$ nanoparticles uniformly distributed and closely attached to the MWCNT surfaces, indicating a strong interaction. This uniform attachment, observed across different samples, implies that $NiFe_2O_4$ is directly crystallized onto the MWCNTs during synthesis, not blended post-synthesis. This is crucial for ensuring the electromagnetic properties of the composite are due to the synergistic effect of the intimately connected components.

### 3.2. Magnetic and Electromagnetic Wave Absorbing Analysis

We conducted magnetic property measurements on nanocomposites synthesized using the microwave-assisted combustion method. The measurements were performed at room temperature (300 K) using a VSM (Figure 3). The samples consisted of pure $NiFe_2O_4$, pure MWCNT, and $NiFe_2O_4$/MWCNT with different concentrations of MWCNT (2wt%, 4wt%, and 6wt%).

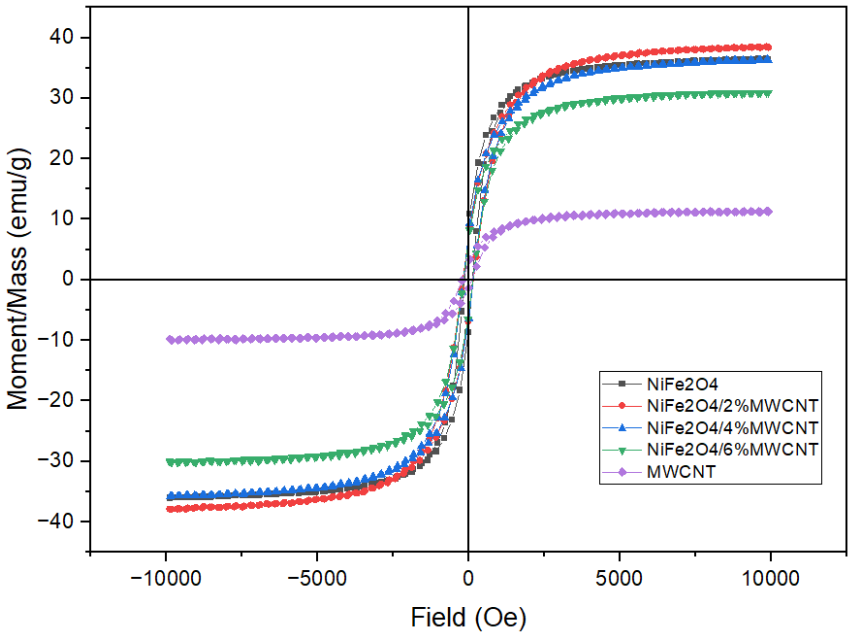


**Figure 3**. The magnetization graph of pure $NiFe_2O_4$, pure MWCNT and $NiFe_2O_4$/MWCNT with different concentration of MWCNT of 2wt%, 4wt% and 6wt%

To determine the magnetic properties, we conducted magnetization measurements on the prepared samples under an applied field of 10 kOe. By obtaining the hysteresis loops of the samples, we extracted relevant magnetic parameters (Table 1). In the case of 2wt%$NiFe_2O_4$/MWCNT, we observed a coercive force ($H_c$) of 172.21 Oe, which is the measure of the resistance of a ferromagnetic material to becoming demagnetized, saturation magnetization ($M_s$) of 38.191 emu/g, representing the maximum magnetization a material can achieve under an external magnetic field, and retentivity ($M_r$) of 6.6954 emu/g, which indicates the residual magnetization left in the material after the external magnetic field is removed. These values indicate the highest magnetic performance among the tested samples (Table 1).

We noticed an increase in the $H_c$, $M_s$, and $M_r$ of the composites as the concentration of MWCNT increased compared to pure $NiFe_2O_4$ (Table 1). However, this trend was followed by a gradual decrease. The decrease in magnetic properties could be attributed to the presence of MWCNT and the resulting structural deformation on the surface of the ferrites. This deformation might occur due to the interaction between transition metal ions and oxygen atoms in the magnetoplumbite lattice, leading to a reduction in the magnetic moment [25].

According to Wesselinowa and Apostolova [26], magnetic anisotropy and particle size play crucial roles in determining the magnetic properties of nanoparticles. The $NiFe_2O_4$ samples have cubic structures and exhibit shape anisotropy. Despite having an average grain size of 1.317 μm (Table 1), which is larger than the critical size for single-domain behaviour (0.4–0.9 μm) as reported by Kamble *et al.* [27], the $NiFe_2O_4$ samples display multidomain behaviour. It was observed that the $NiFe_2O_4$/2wt%MWCNT sample exhibited the highest saturation magnetization. This can be attributed to the significant magnetic mass contribution from $NiFe_2O_4$ and the presence of a catalyst from MWCNT. However, increasing the amount of MWCNT led to a decrease in magnetic mass and subsequently resulted in a decrease in saturation magnetization. In contrast, the MWCNT sample showed weak magnetization in response to the applied magnetic field. It exhibited the lowest magnetic characteristics, with a saturation magnetization of 10.694 emu/g [28].

When MWCNTs were added, magnetic interactions occur between the MWCNTs and the magnetic moments of $NiFe_2O_4$. These interactions have an impact on the overall magnetic behaviour of the composites.

The observed increase in $M_s$ in the $NiFe_2O_4$/2wt%MWCNT composite can be attributed to the enhanced alignment of magnetic moments, which is a result of the interfacial coupling between $NiFe_2O_4$ and MWCNTs. The conductive nature of MWCNTs facilitates the transfer of electrons and spin polarization, thereby enhancing magnetization.

The presence of MWCNTs can introduce structural defects and perturbations in the composite material. These defects may act as pinning sites that influence the movement and reorientation of magnetic moments within the composite. Pinning effects can contribute to increased $H_c$, which represents the resistance to demagnetization.

The $M_s$ of the $NiFe_2O_4$/MWCNT composites decrease at higher MWCNT concentrations (4wt% and 6wt%). This decrease can be attributed to the possible dilution effects caused by the excess MWCNTs. These additional MWCNTs may introduce non-magnetic or weakly magnetic components that disrupt the magnetic interactions within the composite, thereby reducing the overall magnetization.

The addition of MWCNTs has the potential to influence the microstructure of the composites. At lower concentrations, MWCNTs tend to disperse more uniformly throughout the matrix, which is beneficial for achieving optimal enhancement of the composite's magnetic properties due to effective percolation and interaction between MWCNTs and $NiFe_2O_4$ particles. This uniform dispersion supports the maintenance of small average particle sizes, which is crucial for the arrangement and alignment of magnetic moments within the composite. However, as the concentration of MWCNTs increases, challenges emerge due to the potential for agglomeration, which can reduce the effectiveness of dispersion and create non-uniformities in the composite's microstructure. These non-uniformities can impact the overall magnetic performance, leading to variations in magnetic properties, as agglomerated MWCNTs may not provide consistent magnetic interactions across the composite. While the small particle sizes may limit the formation of well-defined domain walls, it is essential to optimize processing conditions to mitigate dispersion issues and enhance the distribution of MWCNTs, even at higher concentrations.

The optimal electromagnetic (EM) wave absorption characteristics of a material are expressed by the equation: $Z_0/Z_{in} = 1$, signifying that the material facilitates easy penetration of the EM wave and absorbs the entire EM energy. Here, $Z_0$ represents the impedance of free space, and $Z_{in}$ is the input impedance at the interface between free space and the absorbing material. The absorption ability of a material, denoted by reflection loss (RL), is defined as per Equation (2):

$$RL(\text{dB}) = 20\log\frac{(Z_{in}-Z_o)}{(Z_{in}+Z_o)} \quad (2)$$

where $Z_{in}$ is the normalized input impedance obtained from the following Equation (3):

$$Z_{in} = Z_o\sqrt{\frac{\mu_r}{\varepsilon_r}}\tanh\left[j\left(\frac{2\pi ft}{c}\right)\sqrt{\mu_r\varepsilon_r}\right] \quad (3)$$

In this context, $f$ represents the frequency of the incident wave, $t$ signifies the thickness of the absorber, $c$ denotes the velocity of EM waves in free space, $\mu_r$ stands for the relative permeability, and $\varepsilon_r$ corresponds to the relative permittivity. Typically, when RL values fall below − 10 dB and − 20 dB, it suggests absorption of more than 90% and 99% of the incident EM wave, respectively. The connection

between the reduction in electromagnetic reflectivity and the percentage of absorbed energy has been explored by Lee [29].

For a more in-depth assessment of the microwave absorption characteristics of the materials, we introduce the attenuation constant (α) in Equation (4) [30]:

$$\alpha = \frac{\sqrt{2\pi f}}{c} \times \sqrt{(\mu"\varepsilon" - \mu'\varepsilon')2 + \sqrt{(\mu"\varepsilon" - \mu'\varepsilon')2 + (\mu'\varepsilon" - \mu"\varepsilon')2}} \quad (4)$$

where, $f$ is the frequency of the electromagnetic wave, $c$ is the speed of light, μ" is imaginary permeability, ε" is imaginary permittivity, μ' is real permeability, and ε' is real permittivity.

The reflection loss was measured in the Ku-band, specifically at 12 GHz to 18 GHz, as depicted in Figure 4(a), with a thickness of 3 mm. Our findings revealed that the microwave absorption capabilities of $NiFe_2O_4$/4wt% MWCNT were enhanced, resulting in a maximum absorption loss of RL −17.58 dB with a bandwidth of 0.45 GHz at a frequency of 12.78 GHz. The presence of a non-magnetic matrix significantly increased microwave absorption, albeit with a no decrease in saturation magnetization [31]. An RL value less than −10 dB corresponded to 90% absorption in the microwave range [32]. Consequently, only the $NiFe_2O_4$/4wt% MWCNT sample could be deemed an effective electromagnetic wave absorber.

Moreover, the improvement in microwave absorption performance could primarily be ascribed to favourable impedance matching ($Z_{in}/Z_o$) and a high value of the attenuation constant (α). Impedance matching was examined in Figure 4(b) to delve deeper into the microwave absorption capabilities of the $NiFe_2O_4$/MWCNT hybrid. The normalized impedance of $NiFe_2O_4$/MWCNT hybrid samples between 12 GHz and 14 GHz was close to 1 and gradually

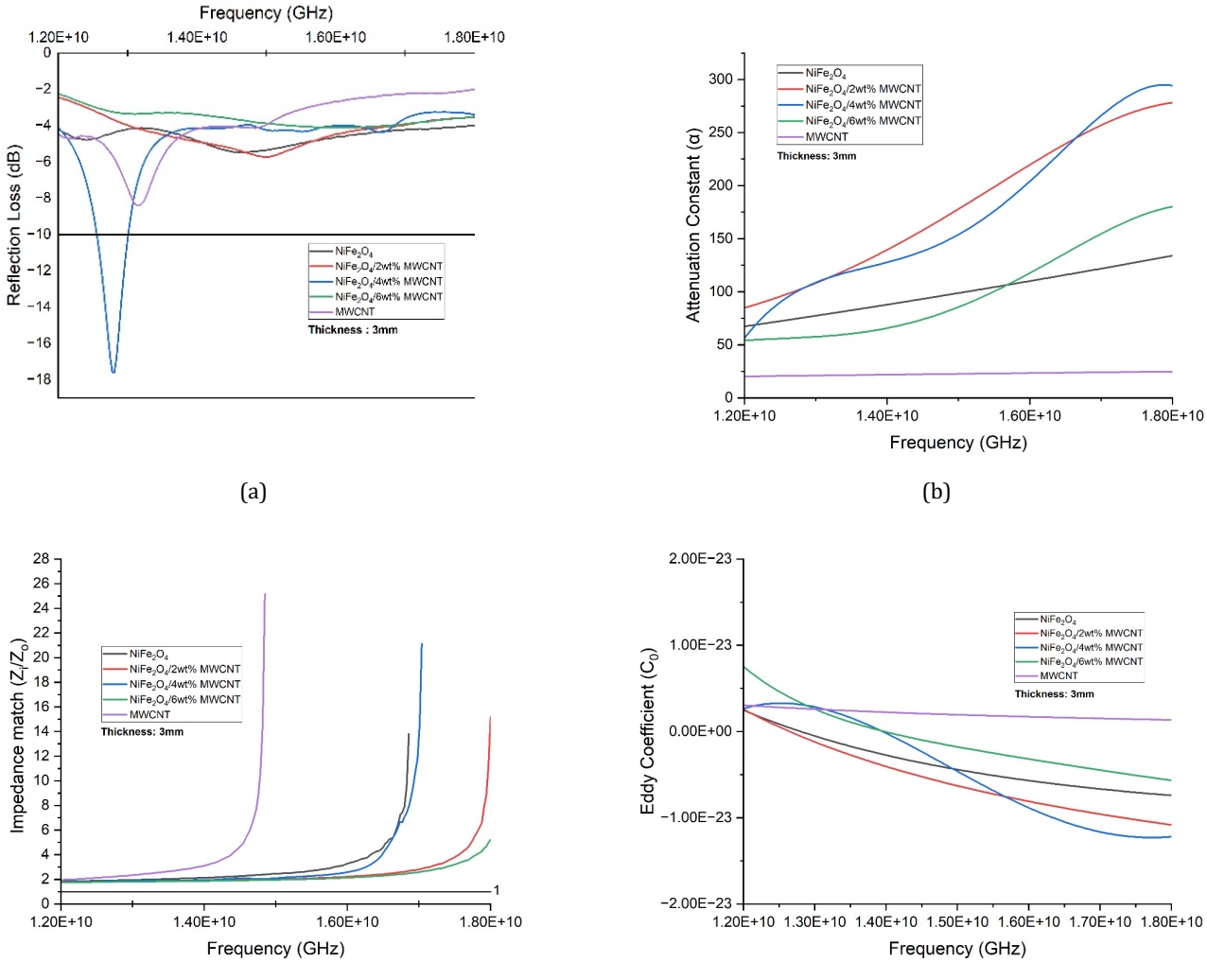


**Figure 4**. Frequency dependency of (a) reflection loss (RL), (b) impedance matching ($Z_{in}/Z_o$), (c) attenuation constant (α) and (d) eddy coefficient ($C_o$) for $NiFe_2O_4$, MWCNT and $NiFe_2O_4$/MWCNT hybrid with different filler contents (2, 4 and 6wt%) and with thickness of $d$ = 3 mm

increased with frequency. In contrast, for pure $NiFe_2O_4$ and MWCNT, the impedance matching diverged more rapidly with increasing frequency. To further investigate the microwave absorption properties, the attenuation constant of the discussed samples was analyzed. In Figure 4(c), the attenuation constants of all pure and hybrid samples are presented as a function of frequency analysed using the formula from reference [30]. All hybrid samples exhibited higher attenuation constants when compared to both pure $NiFe_2O_4$ and MWCNT. Due to their superior impedance matching and higher attenuation constants, the hybrid samples outperformed in microwave absorption. As anticipated, $NiFe_2O_4$/4wt% MWCNT achieved the highest attenuation constant among the samples, validating its highest reflection loss. Consequently, the $NiFe_2O_4$/4wt% MWCNT hybrid sample stands out as the preferred candidate for electromagnetic wave absorption compared to others, as it is the only sample that met the minimum reflection loss target of −10 dB.

In general, magnetic loss arises from domain wall resonance and natural resonance [33] Eddy current and ferromagnetic resonance are contributors to magnetic loss at microwave frequencies. The magnetic loss is solely attributed to the eddy current when $C_o$ remains constant within the specified frequency range. We examined the impact of the eddy current coefficient, by introducing the parameter $C_o = (\mu''(\mu')^{-2f.-1})$ [34]. The frequency-dependent values of $C_o$ are presented in Figure 4(d) to examine the behaviour of the samples. All the samples were observed to be stable, except for $NiFe_2O_4$/4wt% MWCNT, which exhibited fluctuations across the frequency. These findings suggested that eddy current loss played a significant role in magnetic loss within this frequency range [35]. With the exception of the 4wt% sample, all the samples exhibited a decrease in behaviour with increasing frequency, indicating a more consistent pattern along the frequency spectrum, pointing towards the influence of eddy currents. Consequently, the resonance in all samples was primarily attributed to natural ferromagnetic resonance within the specified frequency range [33].

## 4. CONCLUSIONS

In this study, we investigated the synthesis, microstructural characteristics, magnetic properties, and electromagnetic wave absorption capabilities of $NiFe_2O_4$/MWCNT nanocomposites, varying the concentrations of MWCNTs. Utilizing the microwave-assisted combustion (MAC) method with effective dispersion of MWCNTs within the $NiFe_2O_4$ matrix. Microstructural analysis, employing FESEM, confirmed the successful incorporation of MWCNTs, demonstrating their significant impact on hindering grain growth. The average grain size was significantly reduced from 1.317 μm for pure $NiFe_2O_4$ to 0.436 μm for $NiFe_2O_4$/2wt%MWCNT, showcasing the finer grain structure induced by MWCNT entanglement. Particle distribution and size analyses quantified the controlled reduction in average grain size with increasing MWCNT concentrations. The average grain size further decreased to 0.243 μm and 0.270 μm for $NiFe_2O_4$/4wt%MWCNT and $NiFe_2O_4$/6wt%MWCNT, respectively, showing the effective role of MWCNTs as grain boundary migration obstacles. Quantitative magnetic property analyses uncovered a nuanced interplay between MWCNT concentration and composite behaviour. The saturation magnetization (Ms) exhibited a substantial enhancement in the $NiFe_2O_4$/2wt%MWCNT composite, reaching 38.191 emu/g, indicative of effective alignment of magnetic moments facilitated by the interfacial coupling between $NiFe_2O_4$ and MWCNTs. However, a subsequent decrease in Ms at higher MWCNT concentrations (4wt% and 6wt%) was observed, suggesting potential dilution effects and disruptions in magnetic interactions within the composite. Electromagnetic wave absorption investigations revealed $NiFe_2O_4$/4wt%MWCNT as a highly efficient absorber in the Ku-band, with superior impedance matching and a high attenuation constant. The reflection loss (RL) reached a maximum of −17.58 dB at 12.78 GHz, signifying absorption of more than 99% of the incident EM wave in the microwave range. The favourable impedance matching, quantified by $Z_{in}/Z_o$ close to 1, and a high attenuation constant contributed to the superior performance of $NiFe_2O_4$/4wt%MWCNT compared to pure $NiFe_2O_4$ and MWCNT. The improved electromagnetic wave absorption makes the $NiFe_2O_4$/MWCNT composites potential candidates for use in telecommunications, aerospace, and electronics.

## ACKNOWLEDGMENTS

We acknowledge the funding provided for this project by the Ministry of Higher Education (MOHE) Malaysia through the Fundamental Research Grant Scheme (FRGS), Grant No. FRGS/1/2023/STG07/UPM/02/8. The authors are also grateful for access to the measurement facilities offered by the Institute of Nanoscience and Nanotechnology (ION2) and the Department of Physics, Faculty of Science, Universiti Putra Malaysia.

## REFERENCES

[1] S. Sahu, P. P. Mohapatra, H. Karnajit Singh, and P. Dobbidi, "Enhanced microwave absorbing performance of $Sr^{2+}$ substituted Nickel-Cobalt nano ferrite for radar and stealth applications," *Materials Science and Engineering: B*, vol. 294, p. 116514, Aug. 2023, doi: 10.1016/j.mseb.2023.116514.

[2] P. Siva Nagasree, K. Ramji, M. K. Naidu, and T. C. Shami, "X-band radar-absorbing structures based on MWCNTs/NiZn ferrite nanocomposites," *Plastics, Rubber and Composites*, vol. 50, no. 2, pp. 71–82, Feb. 2021, doi: 10.1080/14658011.2020.1836882.

[3] N. Aggarwal and S. B. Narang, "Magnetic characterization of Nickel-Zinc spinel ferrites along with their microwave characterization in Ku band," *Journal of Magnetism and Magnetic Materials*, vol. 513, p. 167052, Nov. 2020, doi: 10.1016/j.jmmm.2020.167052.

[4] P. Smitha *et al.*, "Development of thin broad band radar absorbing materials using nanostructured spinel ferrites," *Journal of Materials Science: Materials*

*in Electronics*, vol. 27, no. 8, pp. 7731–7737, Aug. 2016, doi: 10.1007/s10854-016-4760-6.

[5] J. S. Ghodake, R. C. Kambale, T. J. Shinde, P. K. Maskar, and S. S. Suryavanshi, "Magnetic and microwave absorbing properties of $Co^{2+}$ substituted nickel–zinc ferrites with the emphasis on initial permeability studies," *Journal of Magnetism and Magnetic Materials*, vol. 401, pp. 938–942, Mar. 2016, doi: 10.1016/j.jmmm.2015.11.009.

[6] J. Zhang, R. Shu, C. Guo, R. Sun, Y. Chen, and J. Yuan, "Fabrication of nickel ferrite microspheres decorated multi-walled carbon nanotubes hybrid composites with enhanced electromagnetic wave absorption properties," *Journal of Alloys and Compounds*, vol. 784, pp. 422–430, May 2019, doi: 10.1016/j.jallcom.2019.01.073.

[7] Z. Yue, J. Zhou, L. Li, H. Zhang, and Z. Gui, "Synthesis of nanocrystalline NiCuZn ferrite powders by sol–gel auto-combustion method," *Journal of Magnetism and Magnetic Materials*, vol. 208, no. 1–2, pp. 55–60, Jan. 2000, doi: 10.1016/S0304-8853(99)00566-1.

[8] Y. Köseoğlu, A. Baykal, F. Gözüak, and H. Kavas, "Structural and magnetic properties of $Co_xZn_{1-x}Fe_2O_4$ nanocrystals synthesized by microwave method," *Polyhedron*, vol. 28, no. 14, pp. 2887–2892, Sep. 2009, doi: 10.1016/j.poly.2009.06.061.

[9] T. A. S. Ferreira, J. C. Waerenborgh, M. H. R. M. Mendonça, M. R. Nunes, and F. M. Costa, "Structural and morphological characterization of $FeCo_2O_4$ and $CoFe_2O_4$ spinels prepared by a coprecipitation method," *Solid State Sciences*, vol. 5, no. 2, pp. 383–392, Feb. 2003, doi: 10.1016/S1293-2558(03)00011-6.

[10] S. Singhal, J. Singh, S. K. Barthwal, and K. Chandra, "Preparation and characterization of nanosize nickel-substituted cobalt ferrites ($Co_{1-x}Ni_xFe_2O_4$)," *Journal of Solid State Chemistry*, vol. 178, no. 10, pp. 3183–3189, Oct. 2005, doi: 10.1016/j.jssc.2005.07.020.

[11] Z. Karcıoğlu Karakaş, R. Boncukcuoğlu, İ. H. Karakaş, and M. Ertuğrul, "The effects of heat treatment on the synthesis of nickel ferrite ($NiFe_2O_4$) nanoparticles using the microwave assisted combustion method," *Journal of Magnetism and Magnetic Materials*, vol. 374, pp. 298–306, Jan. 2015, doi: 10.1016/j.jmmm.2014.08.045.

[12] Z. K. Karakaş, R. Boncukçuoğlu, and İ. H. Karakaş, "The effects of fuel type in synthesis of $NiFe_2O_4$ nanoparticles by microwave assisted combustion method," *Journal of Physics: Conference Series*, vol. 707, p. 012046, Apr. 2016, doi: 10.1088/1742-6596/707/1/012046.

[13] İ. H. Karakas, "The effects of fuel type onto the structural, morphological, magnetic and photocatalytic properties of nanoparticles in the synthesis of cobalt ferrite nanoparticles with microwave assisted combustion method," *Ceramics International*, vol. 47, no. 4, pp. 5597–5609, Feb. 2021, doi: 10.1016/j.ceramint.2020.10.144.

[14] T. Mimani and K. C. Patil, "Solution Combustion Synthesis of Nanoscale Oxides and their Composites," *Materials Physics and Mechanics*, vol. 4, no. 2, pp. 134–137, 2001.

[15] B. M. Abu-Zied, "Preparation of cadmium chromite spinel: a combustion approach," *Colloids and Surfaces A: Physicochemical and Engineering Aspects*, vol. 211, no. 1, pp. 27–42, Nov. 2002, doi: 10.1016/S0927-7757(02)00221-2.

[16] S. M. Zanetti, E. I. Santiago, L. O. S. Bulhões, J. A. Varela, E. R. Leite, and E. Longo, "Preparation and characterization of nanosized $SrBi_2Nb_2O_9$ powder by the combustion synthesis," *Materials Letters*, vol. 57, no. 19, pp. 2812–2816, Jun. 2003, doi: 10.1016/S0167-577X(02)01380-0.

[17] X. Yu, C. Zhou, X. He, Z. Peng, and S.-P. Yang, "The influence of some processing conditions on luminescence of $SrAl_2O_4:Eu^{2+}$ nanoparticles produced by combustion method," *Materials Letters*, vol. 58, no. 6, pp. 1087–1091, Feb. 2004, doi: 10.1016/j.matlet.2003.08.022.

[18] N. Kasapoglu, B. Birsöz, A. Baykal, Y. Köseoglu, and M. Toprak, "Synthesis and magnetic properties of octahedral ferrite $Ni_\chi Co_{1-\chi}Fe_2O_4$ nanocrystals," *Open Chemistry*, vol. 5, no. 2, pp. 570–580, Jun. 2007, doi: 10.2478/s11532-007-0005-0.

[19] M. M. Kothawale, R. B. Tangsali, G. K. Naik, and J. S. Budkuley, "Characterization and Magnetic Properties of Nanoparticle $Ni_{1-x}Zn_xFe_2O_4$ Ferrites Prepared Using Microwave Assisted Combustion Method," *Journal of Superconductivity and Novel Magnetism*, vol. 25, no. 6, pp. 1907–1911, Aug. 2012, doi: 10.1007/s10948-012-1510-8.

[20] W. Sami and Z. S. Sadeq, "Synthesis, Characterizations, and Magnetic Properties of Mixed Spinel Mg1-xZnxFe2O4 Ferrites," *Iraqi Journal of Science*, pp. 997–1003, Mar. 2022, doi: 10.24996/ijs.2022.63.3.9.

[21] M. M. M. Zulkimi *et al.*, "Enhancing radar absorption performance of Sr-hexaferrite by hybridization with coiled carbon nanotubes via chemical vapour deposition method," *Diamond and Related Materials*, vol. 137, p. 110118, Aug. 2023, doi: 10.1016/j.diamond.2023.110118.

[22] A. Ghasemi, "The role of multi-walled carbon nanotubes on the magnetic and reflection loss characteristics of substituted strontium ferrite nanoparticles," *Journal of Magnetism and Magnetic Materials*, vol. 330, pp. 163–168, Mar. 2013, doi: 10.1016/j.jmmm.2012.10.033.

[23] S. Abazari *et al.*, "Carbon Nanotubes (CNTs)-Reinforced Magnesium-Based Matrix Composites: A Comprehensive Review," *Materials*, vol. 13, no. 19, p. 4421, Oct. 2020, doi: 10.3390/ma13194421.

[24] A. Mahdy, A. Magdy, E. S. Mosa, and A. Kandil, "effect of MWCNTS on Microstructure, Dry Sliding Wear, and Corrosion Behavior of AA5052/MWCNTS Composite," *Journal of Al-Azhar University Engineering Sector*, vol. 16, no. 61, pp. 1212–1223, Oct. 2021, doi: 10.21608/auej.2021.207682.

[25] J. Jiang, L. Ai, and L. Li, "Multifunctional Polypyrrole/Strontium Hexaferrite Composite Microspheres: Preparation, Characterization, and Properties," *The Journal of Physical Chemistry B*, vol.

113, no. 5, pp. 1376–1380, Feb. 2009, doi: 10.1021/jp808270n.

[26] J. M. Wesselinowa and I. Apostolova, "Size, anisotropy and doping effects on the coercive field of ferromagnetic nanoparticles," *Journal of Physics: Condensed Matter*, vol. 19, no. 40, p. 406235, Oct. 2007, doi: 10.1088/0953-8984/19/40/406235.

[27] R. B. Kamble, V. Varade, K. P. Ramesh, and V. Prasad, "Domain size correlated magnetic properties and electrical impedance of size dependent nickel ferrite nanoparticles," *AIP Advances*, vol. 5, no. 1, Jan. 2015, doi: 10.1063/1.4906101.

[28] H. Hosseini and H. Mahdavi, "Nanocomposite based on epoxy and MWCNTs modified with $NiFe_2O_4$ nanoparticles as efficient microwave absorbing material," *Applied Organometallic Chemistry*, vol. 32, no. 4, Apr. 2018, doi: 10.1002/aoc.4294.

[29] S. M. Lee, *International Encyclopedia of Composites*, vol. 5. VCH, University of Michigan, p. 548, Oct. 04, 1990.

[30] Y. Xiong *et al.*, "Synergistic effect of silica coated porous rodlike nickel ferrite and multiwalled carbon nanotube with improved electromagnetic wave absorption performance," *Journal of Alloys and Compounds*, vol. 802, pp. 364–372, Sep. 2019, doi: 10.1016/j.jallcom.2019.06.174.

[31] D. Sarkar, A. Bhattacharya, P. Nandy, and S. Das, "Enhanced broadband microwave reflection loss of carbon nanotube ensheathed Ni–Zn–Co-ferrite magnetic nanoparticles," *Materials Letters*, vol. 120, pp. 259–262, Apr. 2014, doi: 10.1016/j.matlet.2014.01.089.

[32] S. S. S. Afghahi, M. Jafarian, and Y. Atassi, "Microstructural and magnetic studies on $BaMg_xZn_xX_{2x}Fe_{12-4x}O_{19}$ (X=Zr,Ce,Sn) prepared via mechanical activation method to act as a microwave absorber in X-band," *Journal of Magnetism and Magnetic Materials*, vol. 406, pp. 184–191, May 2016, doi: 10.1016/j.jmmm.2016.01.020.

[33] B. Zhao *et al.*, "Lightweight porous $Co_3O_4$ and Co/CoO nanofibers with tunable impedance match and configuration-dependent microwave absorption properties," *CrystEngComm*, vol. 19, no. 41, pp. 6095–6106, 2017, doi: 10.1039/C7CE01464C.

[34] B. Zhao *et al.*, "1D Cu@Ni nanorods anchored on 2D reduced graphene oxide with interfacial engineering to enhance microwave absorption properties," *CrystEngComm*, vol. 19, no. 44, pp. 6579–6587, 2017, doi: 10.1039/C7CE01439B.

[35] N. Rosdi, R. S. Azis, I. Ismail, N. Mokhtar, M. M. Muhammad Zulkimi, and M. S. Mustaffa, "Structural, microstructural, magnetic and electromagnetic absorption properties of spiraled multiwalled carbon nanotubes/barium hexaferrite (MWCNTs/BaFe12O19) hybrid," *Scientific Reports*, vol. 11, no. 1, p. 15982, Aug. 2021, doi: 10.1038/s41598-021-95332-9.